Uptake of Noncytotoxic Acid-Treated Single-Walled Carbon Nanotubes into the Cytoplasm of Human Macrophage Cells

Alexandra E. Porter,[†,*] Mhairi Gass,[‡] James S. Bendall,[§] Karin Muller,[∥] Angela Goode,[†] Jeremy N. Skepper,[∥] Paul A. Midgley,[¶] and Mark Welland[§]

[†]Department of Materials, Imperial College London, South Kensington, London SW7 2AZ, United Kingdom, [‡]U.K. SuperSTEM, Daresbury Laboratory, Daresbury, Cheshire WA4 4AD, United Kingdom, [§]The Nanoscience Centre, University of Cambridge, 11 J.J. Thompson Avenue, Cambridge CB3 0FF, United Kingdom, [∥]Multiimaging Centre, Department of PDN (Physiology, Development and Neuroscience), Anatomy Building, University of Cambridge, Downing Street, Cambridge CB2 3DY, United Kingdom, and [¶]Department of Materials Science and Metallurgy, University of Cambridge, Pembroke Street, Cambridge CB2 3QZ, United Kingdom

ABSTRACT Water-soluble single-walled nanotubes (SWNTs) are being tested as contrast agents for medical imaging and for the delivery of therapeutically active molecules to target cells. However, before they become used commercially, it will be essential to establish their subcellular distribution and whether they are cytotoxic. Here we characterize uptake of unlabeled, acid-treated, water-soluble SWNTs by human monocyte derived macrophage cells using a combination of Raman spectroscopy and analytical electron microscopy and compare our findings to previous work on unpurified SWNTs. Raman spectroscopy demonstrated that acid-treated SWNTs had a greater number of functional groups on the carbon walls than nontreated SWNT. The acid-treated SWNTs were less aggregated within cells than unpurifed SWNTs. Bundles, and also individual acid-treated SWNTs, were found frequently inside lysosomes and also the cytoplasm, where they caused no significant changes in cell viability or structure even after 4 days of exposure.

KEYWORDS: single-walled carbon nanotube · cytotoxicity · electron microscopy · Raman spectroscopy · nanomedicine

Water-soluble single-walled nanotubes (SWNTs) are being developed as contrast agents in medical imaging and for the delivery of therapeutically active molecules to target cells.[1−3] Development of these SWNTs in diagnostics and therapy will require an understanding of the exact mechanisms of their uptake, the subcellular distribution of SWNTs within cells, and whether they become transformed inside the cell. Further, it is important to establish whether they are cytotoxic before they are used commercially in medical applications.

To be suitable for medical applications, it is necessary first to water solubilize the SWNTs so they are presented to the cell in individual form and second to purify the SWNTs to ensure they are noncytotoxic. One simple technique to solubilize SWNTs is to reflux and dissolve them *via* a multistep acid treatment using both hydrochloric and nitric acid.[4] Nitric acid treatment will alter the surface properties of the SWNTs by generating defects which break the endcaps apart and introducing hydrophilic carboxylic acid groups at the tube ends and, possibly, at defects on the sidewalls.[5] Therefore, it is important to assess the uptake and cytotoxicity of acid-treated SWNTs as they are the precursors for the synthesis of a number of other functionalizations of SWNTs.

Modification of the SWNT surface chemistry will change the interaction of the SWNTs with the lipid bilayer, which may change the uptake into the cell.[6] It is still unclear whether the inherent cytotoxicity of the SWNT samples is due to the structure of the tubular species or the catalyst alone. Acid treatment removes the metal catalyst, which should reduce any potential cytotoxic effect of the SWNTs.[7,8] With the total removal of the metal nanoparticles, we will be able to determine whether a sample consisting of just carbon-based materials causes cell death after prolonged exposure.

Direct imaging of unlabeled, individual SWNTs by electron microscopy is very challenging because it is difficult to distinguish carbon-based nanotubes from carbon-rich organelles due to similarities in their chemical composition and dimension. Visualizing SWNTs inside cells will help us understand how SWNTs enter cells, where they migrate to, and their fate after uptake. Previously, we exposed human monocyte macrophages to unpurified HiPco SWNTs and

*Address correspondence to a.porter@imperial.ac.uk.

Received for review April 27, 2009 and accepted May 11, 2009.

Published online May 21, 2009.
10.1021/nn900416z CCC: $40.75

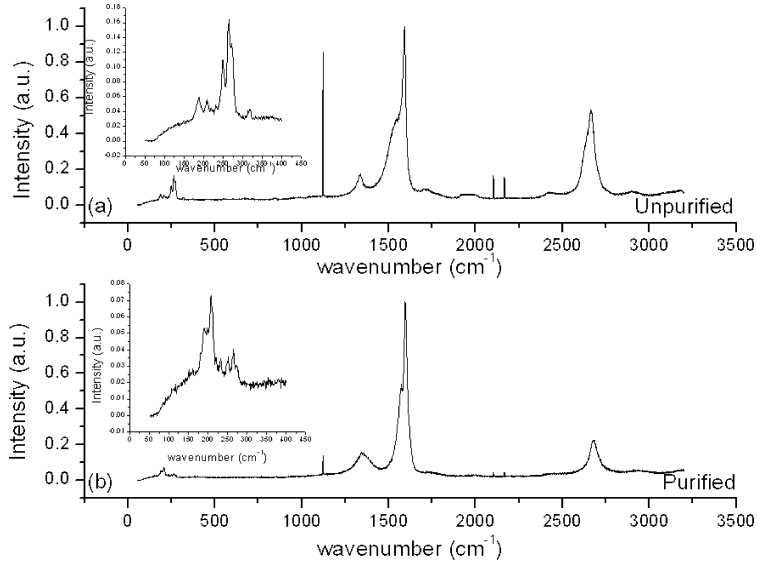

Figure 1. A 514.5 nm excitation Raman spectroscopy of (a) unpurified and (b) purified SWNTs, with relevant RBM modes enlarged as figure inset.

demonstrated that a combination of low-loss energy-filtered transmission electron microscopy (EFTEM) combined with electron energy loss (EEL) spectrum imaging—a method that yields characteristic energy-loss information—enables clear differentiation of SWNTs in the cell. These techniques gave a good image contrast of unstained sections that cannot be achieved using conventional imaging techniques.[9] These images confirmed that unpurified SWNTs localize primarily as bundles within lysosomes but were also seen to enter the cytoplasm and localize within the cell nucleus. They were seen to cause cell mortality in a dose-dependent manner. Visualizing purified water-soluble SWNTs within cells will be particularly challenging as the SWNTs will be more disperse than pristine untreated SWNTs. Furthermore, the iron particles present in unpurified SWNT samples yield more contrast due to the higher atomic number of Fe compared to C so allowing for the SWNT bundles to be more easily identified. Removal of the surface metal catalyst will further complicate imaging of SWNTs inside the cell.

The goal of this study will be to characterize and visualize acid-treated water-soluble SWNTs alone and within human monocyte derived macrophage cells (HMMs). HMMs were chosen as a model as this cell type comprises the first line of defense against foreign organisms or particles and are central to the body's immune responses. Similar to tissue macrophages, they are terminally differentiated and do not proliferate and are more relevant as a macrophage model than immortalized macrophage cell lines. These results will be compared to previous work on unpurified SWNTs.[9] Specifically, we aim to establish the sites they target within the cell, relating the difference in uptake to changes in the chemistry of the SWNT walls, alterations in the diameter distribution, and removal of metallic nanoparticles. Further, we aim to study the cytotoxicity of SWNTs by correlating TEM analysis of changes in the cell structure and morphology on exposure to SWNTs with traditional cell viability assays. Protocols from our previous studies were applied to study these effects in the TEM.[9−11]

RESULTS

Raman Spectroscopy. Raman spectroscopy on SWNTs makes use of the resonance conditions inherent in this one-dimensional material and is sensitive to the electronic structure of the SWNTs being probed.[13] Raman spectroscopy has long been used as a method to determine whether functionalization of SWNTs has occurred as it is sensitive to the electronic structure of the tube walls and therefore sensitive to defect states and changes in hybridization which disrupts the sp^2-bonded network of the SWNT.[14] The relative intensities and peak position of the features in the SWNT Raman spectra will therefore reflect the degree of functionalization of the tube walls. Raman spectroscopy was carried out on material both outside the cells and within the cellular structure. Measurements were taken on both unpurified and purified material, and the tangential mode (TM) bands were peak fitted using a well-known literature method to obtain both peak frequencies and deviation from Lorentzian symmetry to indicate the magnitude of electron−phonon coupling.[15] Due to the weak signal caused by the low quantity of tubular material within each cell, radial breathing modes (RBMs), the frequency of which is dependent on the SWNT diameter, were unobtainable for SWNTs contained within the cell structure. Analysis of the spectra of bulk material arising from excitation with the laser at 514.5 nm (Figure 1a,b) and 633 nm (Figure 2a,b) (thereby accessing two dissimilar SWNT distributions) demonstrated that the RBMs show significant nonlinear intensity changes upon purification but negligible changes in the corresponding positions of the peaks. The peaks most pertinent for observation of functionalization are the D peak, the intensity of which can be related to the level of disorder within the SWNT system, and, to a lesser extent, the G′ (or D*) peak, with Maultzsch *et al.* suggesting that a higher $I_D/I_{G'}$ ratio indicates a higher degree of functionalization, where I indicates the peak intensity of the feature.[16] Both the purified and nonpurified SWNTs showed a small disorder mode (D band) at 1290 cm^{-1} (Figure 1a), but the D band was broader and shifted to higher frequencies for the purified SWNTs,[17] indicating the purification has altered the chemistry of the SWNT and disrupted the pristine nature of the walls so that it resembles a more bulk sp^2-based carbon. The G′ band for the purified sample is smaller relative to the

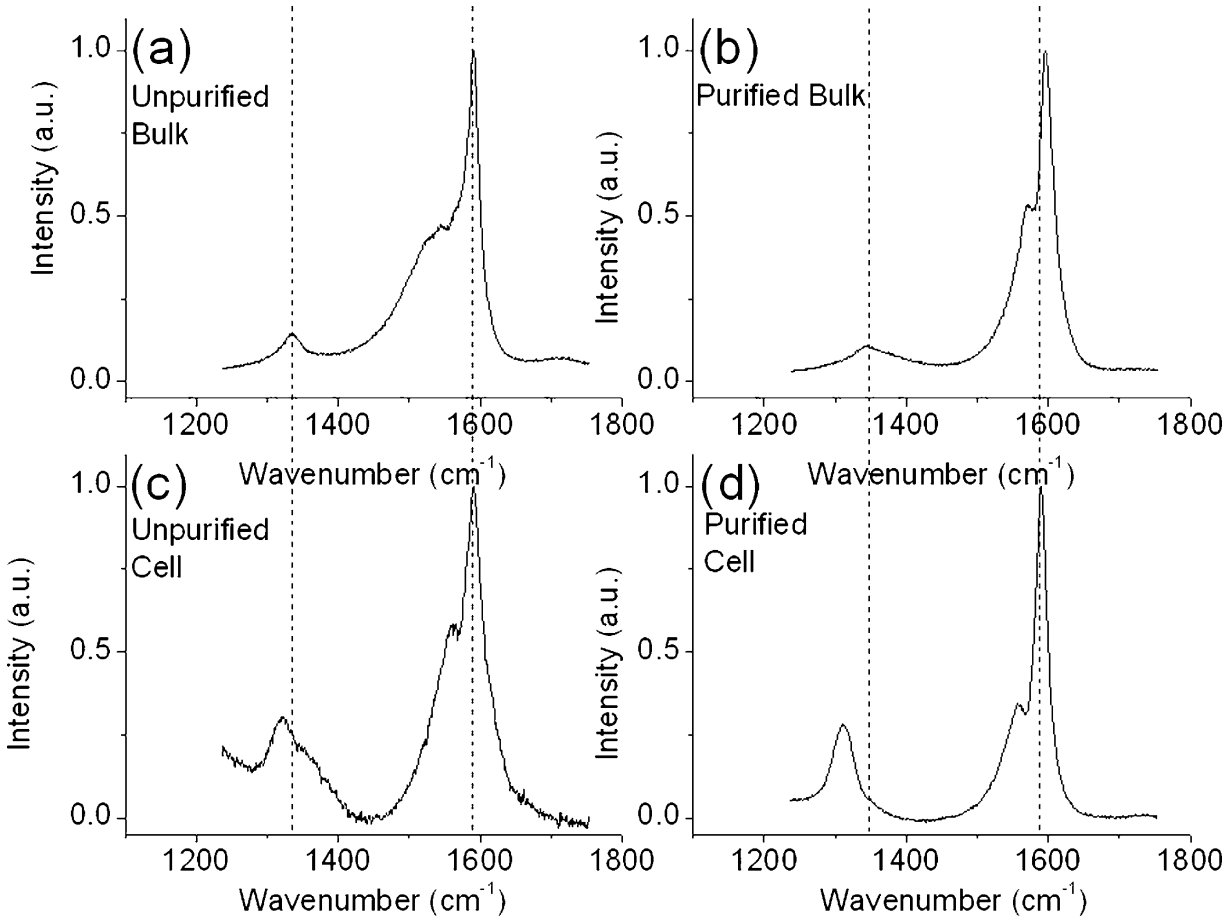

Figure 2. Raman spectroscopy of (a) unpurified SWNTs outside the cell, (b) purified SWNTs outside the cell, (c) unpurified SWNTs inside the cell, and (d) purified SWNTs inside the cell.

G′ band of the unpurified sample. For our experiments with 514.5 nm excitation, the $I_D/I_{G'}$ ratio is *ca.* 0.3 ± 0.05 for unpurified and *ca.* 0.7 ± 0.05 for purified, suggesting the presence of a greater number of functional groups on the carbon walls of the purified SWNTs. Furthermore, the changes in peak intensities observed in the RBMs suggested that our reaction has either damaged the narrower SWNTs, indicated by a reduction in peak intensities at higher wavenumbers, or changed their resonance conditions so that, electronically, they are no longer in resonance with the exciting laser's energy.[18] A diameter distribution skew to a distribution containing wider SWNTs is expected as the narrower SWNTs will be more reactive than the wider SWNTs due to increases in strain energies and reactive sites caused by increases in wall curvature.[19] Upshifts in the G^+ mode could be due to either metal catalyst removal or an increase in the number of electron-accepting functional groups on the SWNT walls caused by the purification process as the G^+ peaks are thought to be diameter-independent, and therefore, such shifts have to be explained in terms of charge transfer. In summary, for the bulk SWNT sample, the purification procedure has altered the Raman spectra of the SWNTs and the procedure has most affected the narrower diameter SWNTs, disrupting their resonance conditions. Due to their increased reactivity, this implies that they are more likely to have been removed during chemical treatment, causing the purified sample to have a distribution of tubes that are of wider diameter compared to as-made. Furthermore, this sample will have fewer nanoparticles of catalyst associated with it.

Comparisons on intra- and extracellular material were carried out on both purified and unpurified materials (Figure 2c,d) with an excitation wavelength of 633 nm. Similarity in the spectra was observed for the purified and unpurified material within the cell. Peak shapes were similar for purified material in either environment, with downshifts observed when the material was encapsulated within the cell. For the unpurified material, there were peak shape and position alterations for intracellular material, notably upshifts for peak positions corresponding to metallic SWNTs, the peaks centered around 1560 cm^{-1}, and a loss of the so-called Breit−Wigner−Fano function, which is related to the degree of electron−phonon coupling within the electronic system. We assign these observations to a number of general phenomena once SWNTs are within cells.

1. Removal of catalyst particles—this is only relevant when comparing unpurified material. For intra-

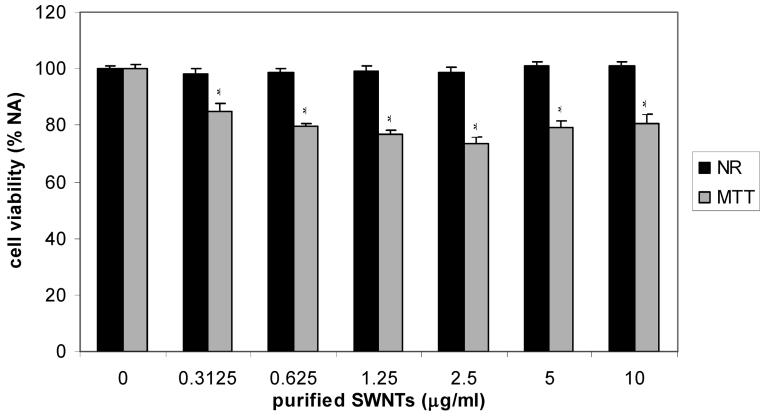

Figure 3. Cytotoxicity of SWNTs. SWNT-treated cells show no significant decrease in viability after 4 days compared to control cells, when measured by the Neutral Red (NR) assay. In contrast, cell viability is significantly decreased at all SWNT concentrations tested when measured by the MTT assay. Values represent the mean ± SE of three experiments in triplicate ($n = 9$). Statistical differences were calculated with Analyse-it software in Excel using a 1-way ANOVA, followed by a LSD post-hoc test; *$p \leq 0.01$.

cellular material, a loss of associated catalyst particles will cause an upshift in the peaks corresponding to metallic SWNTs.

2. Removal of functional groups—only relevant to purified material. Downshifts for the intercellular material could be due to the chemical conditions within the cell where either the functional groups on the cell walls have been altered to minimize their electron-withdrawal effects (for example, changing the inductive effects of the carboxylic groups from the electron-withdrawing −COOH group to the electron-donating $-COO^-$ group in the cell) or the electrons have transferred into the C−C bonds to relax them. In this way, by neutralizing the functional groups on the purified SWNT walls, the SWNTs resemble the unfunctionalized, unpurified material.

3. Debundling of SWNTs within the cells—this can explain the loss of the Breit−Wigner−Fano (BWF) feature for both purified and unpurified material.[15] Relative intensities of the G^- peaks (and hence any associated residual BWF coupling) compared to the G^+ peak are lower for the purified material, suggesting that this has the least bundling within the cellular structure, possibly due to the increased number of functional groups on the tube walls. This is confirmed by the $I_D/I_{G'}$ ratio, which is 0.5 ± 0.1 for unpurified and 0.71 ± 0.01 for purified SWNTs within the cells. Interestingly, both the $I_D/I_{G'}$ ratio and the D peak intensity are greater for SWNTs found within the cell, suggesting that the environment of the cell plays an important role in affecting the surface chemistry of the SWNT. The normalized D peak intensity (I_D/I_G) for material outside the cell was *ca.* 0.1 for both purified and unpurified, whereas for intercellular material, it was *ca.* 0.25 for purified and unpurified.

Cell Viability Assays. The NR assay showed no significant decrease in cell viability at any concentration of SWNTs tested after 4 days exposure (Figure 3). In contrast, all SWNT concentrations tested led to a significant decrease in cell viability when measured by the MTT assay.

Transmission Electron Microscopy. High-magnification lattice imaging confirmed that the graphitic structure of the tubes had been preserved by acid treatment and that the iron catalyst had been removed (Figure 4).

Figure 5a−d illustrates typical images showing the morphology and structure of osmicated sections of necrotic and healthy cells exposed to purified SWNTs after 4 days. In the control, the percentage of cell death was 1.86%. In cells exposed to purified SWNTs, the % cell death was also very low: 2.625 ± 1.07% (mean ± SD, $n = 3$). The major route of cell death appeared to be necrosis. Even in standard BF images, larger bundles of SWNTs could be seen being ingested by HMMs and also in lysosomes and possibly free in the cytoplasm.

To confirm the intracellular localization of individual SWNTs, EEL spectra were acquired from HMMs exposed to SWNTs using unstained cell sections.[9,20] Medium-resolution HAADF-STEM appears to show SWNTs bundles within the cell (Figure 6a). Low-loss EEL spectrum images were taken from the boxed-out region in Figure 6c. A low-loss EELS spectra for SWNTs in the cell and the cell are shown in Figure 6b. A nonlinear least-squares (NNLS)[9] fit was applied to the $(\sigma + \pi)$[20] bulk plasmon peak and the peak position extracted. The position of the plasmon maximum ranged from 17.5 eV from the cell to 21.5 eV from the intracellular SWNTs, the apparently low energy values recorded are a result of the thin nature of the sections but are still comparable.[9,21] Hence, by mapping the peak position (Figure 6c), enhanced contrast due to SWNTs was possible. High-resolution lattice imaging also confirmed the presence of SWNTs within the cell (Figure 6d).

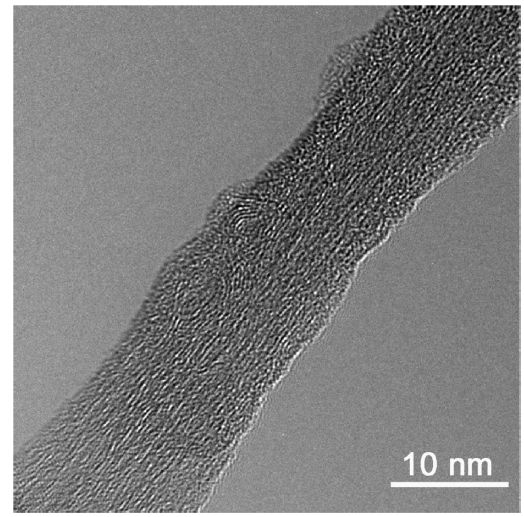

Figure 4. High-resolution bright field image of purified SWNTs showing the lattice spacing of individual carbon layers.

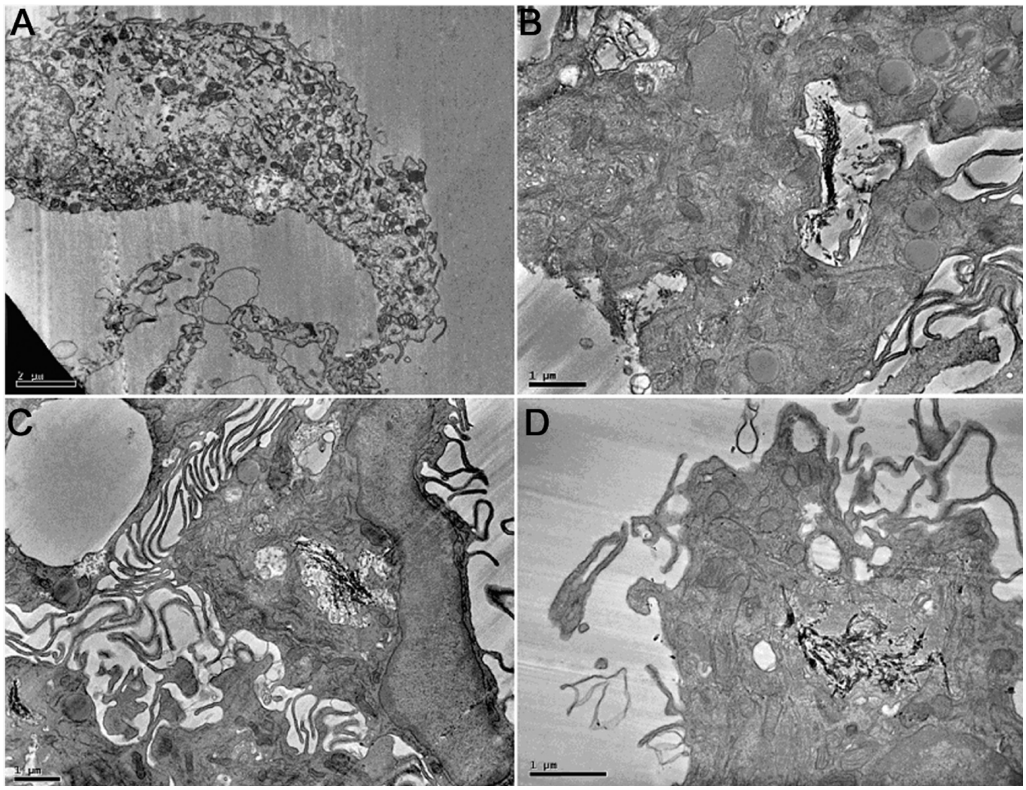

Figure 5. Bright field TEM images of (a) a necrotic cell, (b) phagocytosis of SWNTs, and SWNTs located within (c) lysosomes and (d) the cytoplasm.

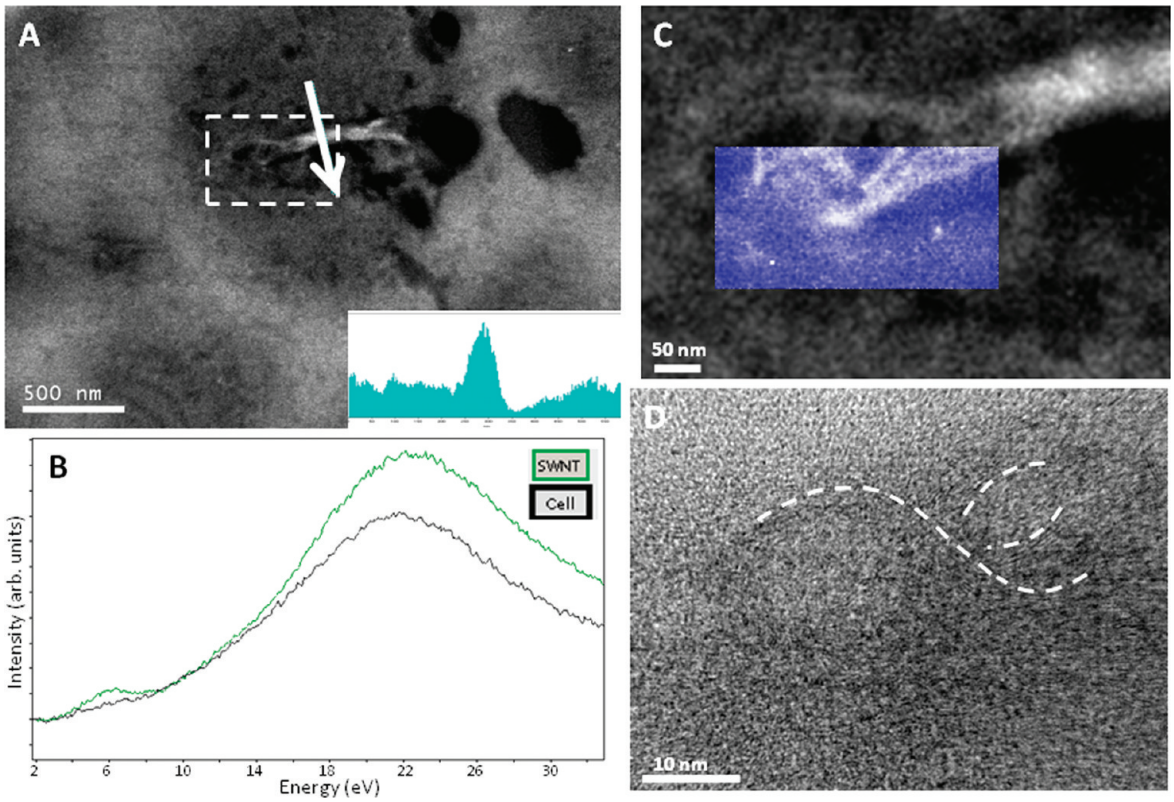

Figure 6. (a) HAADF-STEM image of SWNT bundles within the cytoplasm of an unstained cell. The white box shows area analyzed by low-loss EELS spectroscopy. The inset shows an intensity profile taken along the direction of the arrow; the increase in intensity at the location of the SWNTs is evident. Low-loss EELS spectra for SWNTs in the cell (green) and the cell (gray) are shown in (b). The $\pi-\pi^*$ transition at ~6 eV is seen clearly only in the spectrum taken from the SWNT bundle; it also exhibits a higher bulk plasmon energy. (c) Map showing the change in the plasmon peak position. Range from 17.5 (dark blue) to 21.5 eV (white). Contrast due to SWNTs can be seen that is not identified in conventional imaging. (d) High-resolution lattice image of intracellular SWNTs. Some of the SWNTs have been indicated with a white dotted line as the contrast is weak.

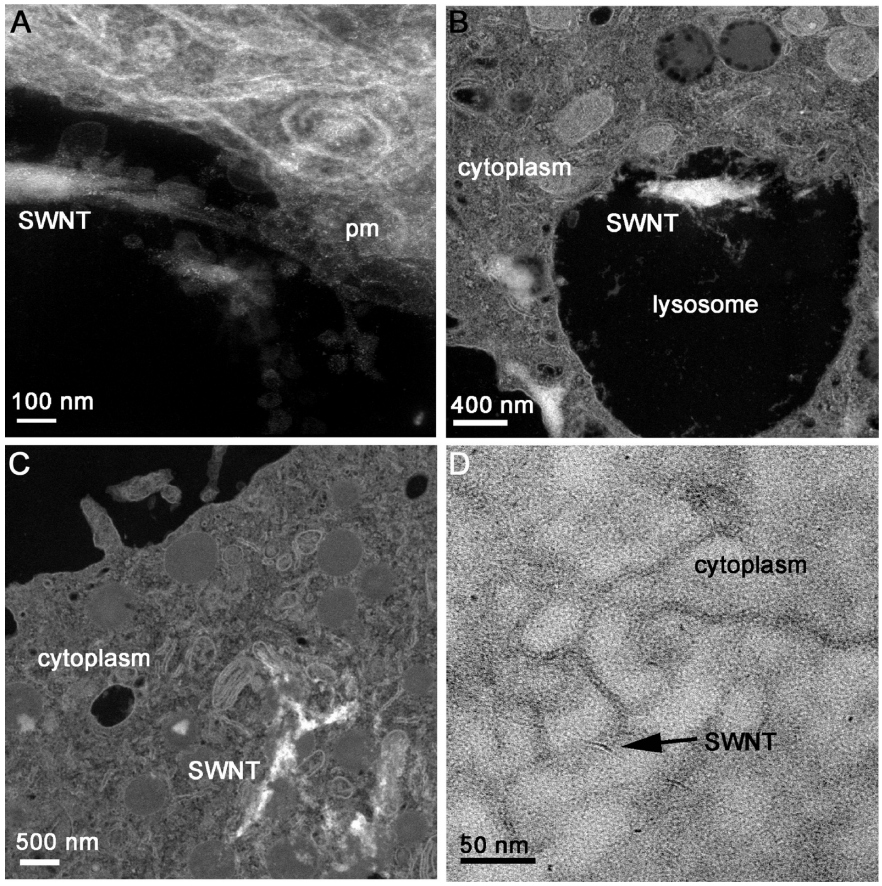

Figure 7. Interactions of SWNTs with cell organelles in osmicated cells. HAADF-STEM images of (a) bundles of SWNTs aligned parallel to and fusing with the plasma membrane. (b) Bundles of SWNTs within a lysosome. (c) Bundles of SWNTs within the cytoplasm. (d) Zero-loss EFTEM map of an individual SWNT within the cytoplasm.

In order to highlight contrast from cell organelles, sections of osmicated cells were studied. High-angle annular dark field (HAADF)-STEM illustrated SWNTs aligned parallel to and fusing with the plasma membrane (Figure 7a). Bundles of SWNTs were also found within lysosomes (Figure 7b) and frequently within the cytoplasm (Figure 7c). Zero-loss EFTEM images also illustrated individual SWNTs present within the cytoplasm of cells (Figure 7d).

DISCUSSION

In summary, we have successfully produced purified SWNTs *via* a multistep acid treatment using both hydrochloric and nitric acid.[4] Raman and TEM characterizations have shown that our purification procedure produces a sample of functionalized SWNTs that contains much fewer catalyst nanoparticles. The NR assay confirmed that acid-treated SWNTs cause no significant changes in cell viability to HMMs. In comparison, the MTT assays showed a significant difference. It is well-established that this difference arises because SWNTs can give false positives with the MTT assay.[22] TEM analysis of the localized effects of SWNTs on cell health also confirmed that cell death was very low after 4 days. In contrast, exposure of cells to unpurified SWNTs has been shown in our previous study to result in a significant decrease in cell viability (Figure SE1 in Supporting Information[9]). These findings support previous observations that decreased cytotoxicity of the purified SWNTs arises as the iron catalyst particles generate free radicals (*via* a Fenton-like reaction) and cause lipid peroxidation at the plasma membrane.[7,8,23]

Decreased cytotoxicity of the acid-treated SWNTs compared to unpurified SWNTs may also arise due to increased surface derivatization.[24] Molecular dynamics simulations have shown that uptake of SWNTs into the cell is modified by changing their surface derivatization.[6] Here we show that there are a greater number of functional groups and defects associated with the acid-treated SWNT walls. We were able to directly visualize acid-treated SWNTs entering different intracellular sites than untreated SWNTs,[9] where negatively charged SWNTs localize more frequently within the cytoplasm of the cell. These findings were supported by Raman measurements where the purified SWNTs were more disperse within the cell. Our current findings correlate with confocal microscopy results, illustrating that fluorescently labeled derivatized SWNTs localize primarily within the cytoplasm[25−27] and the perinuclear region of the cell.[28] Further work is needed to address mechanisms by which the SWNTs entered the cytoplasm, that is, whether they were trafficked intracellularly to this site or whether they passively diffused across the plasma membrane.

Differences in uptake of the acid-treated and unpurified SWNTs may also relate to differences in their aspect ratios. Acid-treated SWNTs are purified in strong acidic conditions, making them defective. This will shorten the length of the SWNTs,[29] which may modify the pathway by which they enter the cell. DNA-wrapped SWNTs shorter than about 200 nm readily enter the cytosol of human lung cells and so may pose an increased risk to health.[30] Here we show that acid-treated SWNTs more frequently enter the cytoplasm of the cell, but that the acid-treated SWNTs are less cytotoxic to the cell than longer untreated SWNTs, again highlighting the role of the iron catalyst in provoking cytotoxicity.

Functionalized, water-soluble SWNTs such as ammonium (NH_3^+) SWNTs are being developed for drug, vaccine, gene delivery, and as contrast agents in medical

imaging.[27] Many of these functionalization strategies require that the SWNTs are oxidized using strong acid treatment. The carboxylates on the surface of the SWNTs are then used to incorporate a variety of other groups to improve the SWNT solubility. Hence acid treatment is an ideal starting platform to test and study the uptake and cytotoxicity of functionalized SWNTs.

Our data show that this medically relevant class of SWNTs is noncytotoxic to the cell and can target the cell cytoplasm. This platform can be used in future investigations to guide studies to assess uptake of more medically relevant classes of functionalized SWNTs being developed as vehicles for the delivery of therapeutic and diagnostic agents.

MATERIALS AND METHODS

Preparation of Single-Walled Nanotubes. Owing to their widespread use and easy commercial availability, purified SWNTs (purified HiPco, 15 wt % ash content) were purchased from Carbon Nanotechnologies. These SWNTs were produced by chemical vapor deposition (CVD) by means of the HiPco process. This process produces SWNTs with a Gaussian distribution of diameters, with a maximum peak around 0.9−1.2 nm. SWNTs were fully characterized by high-resolution (HR) TEM and EELS prior to exposure, which showed bundles of SWNTs decorated with iron catalyst particles and also onion-like structures around iron particles and confirmed they were graphitic-like carbon.

A wet chemical technique was used to remove the catalyst and nontubular carbon species. This multistep process involving soft oxidation of the metal particles and subsequent removal of metal oxides is effective at removing both carbonaceous and catalytic impurities. As-prepared SWNTs were refluxed in concentrated HNO_3 for 3 h at 110 °C to allow the acid to preferentially attack the more reactive carbon sites such as the SWNT caps due to their high curvature, sidewall defects, and the amorphous carbons surrounding the catalyst particles. After the solution was filtered under vacuum, washed with water, and dried at 110 °C for 6 h, the sample was oxidized in static air at 350 °C for 30 min to burn off the amorphous carbon and to oxidize the surface of the metal catalyst particles. The powder was heated under reflux in concentrated HCl for 6 h at 110 °C to dissolve the metal oxide particles and finally filtered under vacuum, washed with water, and dried at 110 °C for 6 h. Following purification, the SWNTs' purification quality was checked using electron microscopy and Raman spectroscopy. Raman spectroscopy was performed on a Renishaw spectrometer through a 50× objective and in the backscattering geometry. An air-cooled Ar^+ laser at 514.5 nm was used for excitation. The SWNT material was used in the form of thick bundles deposited on a silicon substrate, so the spectra acquired were characteristic of the overall SWNT distribution. Care was taken to limit the laser power to ensure that local heating effects were minimized within the SWNT bundles.

Cell Culture Study. The detailed methods used for the *in vitro* cell culture study and electron microscopy have been published previously.[10] In summary, human monocyte derived macrophages (HMMs) were treated with purified SWNTs for 4 days at concentrations of 0−10 μg/mL using a serum-free medium (Macrophage-SFM, Invitrogen). SWNTs were dispersed in sterile water by ultrasonication for 10 min at a concentration of 1 g/L to break up any SWNT bundles. Subsequently, SWNT suspension was diluted in MØ-SFM medium and mixed thoroughly. The purified SWNTs were found to disperse well in the cell culture medium, so no additional dispersing agent was required. Unpurified SWNTs were dispersed in tetrahydrofuran (THF), and bundles were broken up by ultrasonication for 10 min. SWNTs were freshly suspended in the THF by sonicating for 30 min. The suspension was immediately mixed into a serum-free cell culture medium using a pipet. No dispersing reagent (such as a surfactant) was used to break up the as-prepared SWNT bundles so as to maintain the intrinsic properties of the SWNTs. Following the incubation with SWNTs for 4 days, cell viability was measured using the Neutral Red (NR) (3-amino-7-dimethylamino-2-methylphenazine hydrochloride) and MTT [3-(4,5-dimethylthiazol-2-yl)-2,5-diphenyltetrazolium bromide] assays. In both assays, cytotoxicity is a relative measure, where the control sample is set to represent 100% cell viability. For cell viability assays, statistics were calculated using Analyse-it software in Excel. Groups were compared using a 1-way ANOVA, followed by the LSD post-hoc test; $*p \leq 0.01$.

Electron Microscopy. TEM studies were performed at a concentration of 5 μg/mL in accordance with previous studies.[10] Following exposure, washed cell monolayers were fixed with 4% gluteraldehyde in PIPES buffer (0.1 M, pH 7.4) for 1 h at 4 °C. Then, cells were treated with graded solutions of ethanol (70, 95, and 100%) for 5 min in each solution. Samples were then prepared in and in the absence of osmication and infiltrated under vacuum in quetol resin (Agar Scientific, UK) for 3 days. For electron microscopy studies, cells were sectioned with an ultramicrotome at 40 nm for scanning transmission electron microscopy combined with electron energy-loss spectroscopy (STEM -EELS) and at 70 nm for high-angle annular dark field (HAADF)-STEM imaging. Selected samples were post-stained with uranyl acetate and lead citrate for 5 min in each to enhance contrast from cell membranes. These heavy metal stains obscure contrast from SWNTs inside the cell, making it difficult to image and characterize the chemistry of individual SWNTs. Therefore, in order to image individual SWNTs, unstained cell sections were also imaged. The morphology of the cells in stained sections was then compared with unstained sections. Contrast from intracellular SWNTs was then achieved using analytical electron energy-loss spectrum imaging according to previously published methods.[9]

Changes in cell morphology upon exposure to SWNTs were assessed by comparing the structure and morphology of exposed and unexposed cells which had been bulk stained with osmium tetroxide and post-stained with lead citrate and uranyl acetate to enhance contrast from cell organelles. A sample of 800 cells were analyzed in each group with three replicates. Apoptotic and necrotic cells were identified by comparing cell morphology to reference images from previous studies.[11] Apoptotic cells were characterized as shrunken, containing vacuoles in a condensed cytoplasm, and showing heavily capped chromatin. Necrotic cells were more electron-lucent than normal or apoptotic cells, and their cytoplasmic and nuclear contents appeared to be leached out.

All TEM observations were made by analyzing several areas from three specimens. Bright field imaging was performed on the Jeol 200 TEM operatred at 120 kV. Energy-filtered transmission electron microscopy (EFTEM) studies were performed on a Philips CM300 operated at 200 kV using a 10 μm objective aperture to optimize spatial resolution.[12] To optimize contrast, zero-loss images of nonstained sections were taken using a 3 eV energy window. High-resolution STEM and EELS were performed at the UK SuperSTEM laboratory on a VG HB501 dedicated aberration corrected STEM operated at 100 keV and fitted with a Nion second generation spherical aberration corrector and a Gatan Enfina electron energy-loss spectrometer. The convergence semiangle of the electron probe was 24 mrad for both imaging and spectroscopy. Medium-resolution HAADF-STEM of stained sections was performed on an FEI Tecnai F20 operated at 200 kV using a 30 μm condenser aperture and a camera length of 150 mm.

Raman Microscopy. For Raman spectroscopy, cells (macrophages, macrophages exposed to unpurified SWNTs, and macrophages exposed to acid-treated SWNTs) were sectioned at 1 μm with an ultramicrotome and mounted on glass slides. Raman spectroscopy was performed on a Renishaw spectrometer through a 50× objective in the backscattering geometry, and

samples were excited with an air-cooled Ar^+ laser operated at 514.5 nm (2.41 eV). Care was taken to prevent heating effects taking place in the SWNT sample by keeping the laser energy low.

Acknowledgment. Financial support was provided by the IRC in Nanotechnology, Cambridge, UK, The Isaac Newton Trust, EPSRC, Royal Academy of Engineering, and the Oppenheimer Research Trust. The Multiimaging Centre was established with funding from the Wellcome Trust.

Supporting Information Available: Figures SE1 compares the cytotoxicity of purified to unpurified SWNTs using the neutral red and MTT assays. This material is available free of charge *via* the Internet at http://pubs.acs.org.

REFERENCES AND NOTES

1. Kam, N. W.; O'Connell, M.; Wisdom, J. A.; Dai, H. Carbon Nanotubes as Multifunctional Biological Transporters and Near-Infrared Agents for Selective Cancer Cell Destruction. *Proc. Natl. Acad. Sci. U.S.A.* **2005**, *102*, 11600–11605.
2. Jin, H.; Heller, D. A.; Sharma, R.; Strano, M. A. Size-Dependent Cellular Uptake and Expulsion of Single-Walled Carbon Nanotubes: Single Particle Tracking and a Generic Uptake Model for Nanoparticles. *ACS Nano* **2009**, *3*, 149–158.
3. Bhirde, A. A.; Patel, V.; Gavard, J.; Zhang, G.; Sousa, A. A.; Masedunskas, A.; Leapman, R. D.; Weigert, R.; Gutkind, J. S.; Rusling, J. F. Targeted Killing of Cancer Cells *In Vivo* and *In Vitro* with EGF-Directed Carbon Nanotube-Based Drug Delivery. *ACS Nano* **2009**, *3*, 307–316.
4. Kajiura, H.; Tsutsui, S.; Huang, H.; Murakami, Y. High-Quality Single-Walled Carbon Nanotubes from Arc-Produced Soot. *Chem. Phys. Lett.* **2002**, *364*, 586–592.
5. Banerjee, S.; Hemraj-Benny, T.; Wong, S. Covalent Surface Chemistry of Single-Walled Carbon Nanotubes. *Adv. Mater.* **2005**, *17*, 17–29.
6. Lopez, C. F.; Nielsen, S. O.; Moore, P. B.; Klein, M. L. Understanding Nature's Design For a Nanosyringe. *Proc. Natl. Acad. Sci. U.S.A.* **2004**, *101*, 4431–4434.
7. Nimmagadda, A.; Thurston, K.; Nollert, M. U.; McFetridge, P. S. Chemical Modification of SWNT Alters *In Vitro* Cell−SWNT Interactions. *J. Biomed. Mater. Res. A* **2006**, *1 76*, 614–625.
8. Pulskamp, K.; Diabate, S.; Krug, H. Carbon Nanotubes Show no Sign of Acute Toxicity but Induce Intracellular Reactive Oxygen Species in Dependence on Contaminants. *Toxicol. Lett.* **2007**, *168*, 58–74.
9. Porter, A. E.; Gass, M.; Muller, K.; Skepper, J. N.; Midgley, P. A.; Welland, M. Direct Imaging of Single-Walled Carbon Nanotubes in Cells. *Nat. Nano.* **2007**, *2*, 713–717.
10. Porter, A. E.; Muller, K.; Skepper, J.; Midgley, P.; Welland, M. Uptake of C_{60} by Human Macrophages, Its Localization and Implications for Toxicity: Studied by High Resolution Electron Microscopy. *Acta Biomater.* **2006**, *2*, 409–419.
11. Hardwick, S. J.; Hegyi, L; Clare, K.; Law, N. S.; Carpenter, K. H.; Mitchinson, M. J.; Skepper, J. N. Apoptosis in Human Monocyte-Macrophages Exposed to Oxidized Low Density Lipoprotein. *J. Pathol.* **1996**, *179*, 294–302.
12. Krivanek, O. L.; Kundmann, M. K.; Kimotok, K. Spatial Resolution in EFTEM Maps. *J. Microsc.* **1995**, *180*, 277–287.
13. Ilie, A.; Bendall, J. S.; Roy, D.; Philip, E.; Green, M. L. H. Effects of KI Encapsulation in Single-Walled Carbon Nanotubes by Raman and Optical Absorption Spectroscopy. *J Phys. Chem. B* **2006**, *110*, 138–148.
14. Graupner, R. Raman Spectroscopy of Covalently Functionalized Single-Wall Carbon Nanotubes. *J. Raman Spectrosc.* **2007**, *38*, 673–683.
15. Kawamoto, H.; Uchida, T.; Kojima, K.; Tachibana, M. The Feature of the Breit−Wigner−Fano Raman Line in DNA-Wrapped Single-Wall Carbon Nanotubes. *J. Appl. Phys.* **2006**, *99*, 094309.
16. Maultzsch, J.; Reich, S.; Thomsen, C.; Webster, S.; Czerw, R.; Carroll, D.; Vieira, S. M. C.; Birkett, P. R.; Regoet, C. A. Raman Characterization of Boron-Doped Multiwalled Carbon Nanotubes. *Appl. Phys. Lett.* **2002**, *81*, 2647–2649.
17. Jorio, A.; Pimenta, M. A.; Souza Filho, A. G.; Saito, R.; Dresselhaus, G.; Dresselhaus, M. S. Characterizing Carbon Nanotube Samples with Resonance Raman Scattering. *New J. Phys.* **2003**, *5*, 1–17.
18. Rao, A. M.; Richter, E.; Bandow, S.; Chase, B.; Eklund, P. C.; Williams, K. A.; Feng, S.; Subbaswamy, K. R.; Menon, M.; Thess, A.; *et al.* Diameter-Selective Raman Scattering from Vibrational Modes in Carbon Nanotubes. *Science* **1997**, *275*, 187.
19. Park, S.; Srivastava, D.; Cho, K. Generalized Chemical Reactivity of Curved Surfaces: Carbon Nanotubes. *Nano Lett.* **2003**, *3*, 1273–1277.
20. Saito, Y.; Shinoara, H.; Ohshita, A. Bulk Plasmons in Solid C_{60}. *Jpn. J. Appl. Phys.* **1991**, *30*, 1068–1070.
21. Bursill, L. A.; Stadelmann, P. A.; Peng, J. L.; Prawer, S. Surface Plasmon Observed for Carbon Nanotubes. *Phys. Rev. B* **1994**, *49*, 2882–2887.
22. Wörle-Knirsch, J. M.; Pulskamp, K.; Krug, H. F. Opps they did it again! Carbon Nanotubes Hoax Scientists in Cell Viability Assays. *Nano Lett.* **2006**, *6*, 1261–1268.
23. Kagan, V. E.; Tyurina, Y. Y.; Tyurin, V. A.; Konduru, N. V.; Potapovich, A. I.; Osipov, A. N.; Kisin, E. R.; Schwegler-Berry, D.; Mercer, R.; Castranova, V; *et al.* Direct and Indirect Effects of Single Walled Carbon Nanotubes on RAW 264.7 Macrophages: Role of Iron. *Toxicol. Lett.* **2006**, *1*, 88–100.
24. Sayes, C. M.; Liang, F.; Hudson, J. L.; Mendez, J.; Guo, W.; Beach, J. M.; Moore, V. C.; Condell, D.; West, J. L.; Billups, W. E.; *et al.* Functionalization Density Dependence of Single-Walled Carbon Nanotubes Cytotoxicity *In Vitro*. *Toxicol. Lett.* **2006**, *161*, 135–142.
25. Isobe, H.; Tanaka, T.; Maeda, R.; Noiri, E.; Solin, N.; Yudasaka, M.; Iijima, S.; Nakamura, E. Preparation, Purification, Characterization and Cytotoxicity Assessment of Water-Soluble, Transition-Metal Free Carbon Nanotube Aggregates. *Angew. Chem., Int. Ed.* **2006**, *45*, 6676–6680.
26. Pantarotto, D.; Singh, R.; McCarthy, D.; Efhardt, M.; Briand, J. P.; Prato, M.; Kostarelos, K.; Bianco, A. Functionalized Carbon Nanotubes for Plasmid DNA Gene Delivery. *Angew. Chem., Int. Ed.* **2004**, *43*, 5242–5246.
27. Dumortier, H.; Lacotte, S.; Pastorin, G.; Marega, R.; Wu, W.; Bonifazi, D.; Briand, J. P.; Prato, M.; Muller, S.; Bianco, A. Functionalized Carbon Nanotubes are Non-Cytotoxic and Preserve the Functionality of Primary Immune Cells. *Nano Lett.* **2006**, *7*, 1522–1528.
28. Kostarelos, K.; Lacerda, L.; Pastorin, G.; Wu, W.; Wieckowsk, S.; Luangsivilay, J.; Godefroy, S.; Pantarotto, D.; Briand, J. P.; Muller, S.; et al. Cellular Uptake of Functionalised Carbon Nanotubes is Independent of Functional Group and Cell Type. *Nat. Nano* **2007**, *2*, 108–113.
29. Liu, J.; Rinzler, A. G.; Dai, H.; Hafiier, J. H.; Bradley, R. K.; Boul, P. J.; Lu, A.; Iverson, T.; Shelimov, K.; Huffinan, C. B.; et al. Fullerene Pipes. *Science* **1998**, *280*, 1253–1255.
30. Becker, M. L.; Fagan, J. A.; Gallant, N. D. Length-Dependent Uptake of DNA-Wrapped Single-Walled Carbon Nanotubes. *Adv. Mater.* **2007**, *19*, 939–945.